Biointerface Research in Applied Chemistry
Open-Access Journal (ISSN: 2069-5837)

Article
Volume 16, Issue 3, 2026, 78
https://doi.org/10.33263/BRIAC163.078

Modified Iron-Coated Hard Clam Shells for Phosphate Adsorption through Up-flow Column Reactor: Physicochemical Approach to Water Purification Analysis

Norzainariah Abu Hassan [1,*], Noorul Hudai Abdullah [2,*], Nur Husna Muslim [1], Nur Syazrena Amyza Zainal [3]

[1] Faculty of Engineering Technology, Universiti Tun Hussein Onn Malaysia, Hab Pendidikan Tinggi Pagoh, Km 1, Jalan Panchor, 84600 Muar, Johor, Malaysia; hn230002@student.uthm.edu.my (N.A.H.); hn230037@student.uthm.edu.my (N.H.M.);
[2] Neo Environmental Technology, Center for Diploma Studies, Universiti Tun Hussein Onn Malaysia, Pagoh Education Hub, 84600 Pagoh, Johor, Malaysia; noorul@uthm.edu.my (N.H.A.);
[3] Multi Tank Terminal Sdn. Bhd., PT 64374, Jalan Perigi Nenas 8/8, Taman Perindustrian Pulau Indah, Pulau Indah, Wesport, 42920 Pelabuhan Klang, Selangor, Malaysia; mmwwtp@multitank.com.my (N.S.A);
* Correspondence: hn230002@student.uthm.edu.my (N.A.H.); noorul@uthm.edu.my (N.H.A.);

Received: 7.02.2026; Accepted: 19.05.2026; Published: 15.06.2026

Abstract: Phosphorus contamination is a major contributor to eutrophication in aquatic systems, requiring an effective and sustainable removal method. This study investigates the use of modified iron-coated hard clam shells as a sustainable adsorbent for phosphate removal in an up-flow column. The effect of flow rate, initial phosphate concentration, and bed depth on adsorption performance was evaluated. A maximum phosphate removal efficiency of 65.1% was achieved at a bed depth of 8 cm. The breakthrough data were analyzed using Modified Mass Transfer Factor (MMTF), Thomas, and Bed Depth Service Time (BDST). The BDST model showed a linear relationship between bed depth and service time, indicating predictable column performance. The Thomas model showed a reasonable fit to the experimental data ($R^2 = 0.84 – 0.99$), with adsorption capacity increasing with bed depth. Negative Thomas parameters observed at lower bed depths were interpreted cautiously, as they may reflect limitations in model fitting under early breakthrough conditions. The MMTF model further indicated that mass-transfer resistance becomes more significant at greater bed depths. This study shows that modified hard clam shells have potential as a sustainable adsorbent for phosphate removal, particularly under continuous flow conditions. The use of waste-derived materials also supports resource recovery and environmental sustainability.

Keywords: phosphate removal; modified iron-coated hard clam shells; adsorption; up-flow column reactor.

1. Introduction

The accumulation of phosphorus in aquatic environments is a major factor driving eutrophication, a serious environmental concern. Elevated phosphate levels, commonly originating from agricultural runoff, industrial waste, and domestic wastewater, promote algal blooms, leading to oxygen depletion and the release of harmful toxins [1]. This effect disrupts aquatic ecosystems, reduces biodiversity, and negatively impacts economic activities such as

fisheries [2]. Therefore, effective phosphorus strategies are essential to protect water quality, maintain the ecosystem balance, and ensure safe water use.

Increasing pollution in the environment has led many countries to implement stricter discharge regulations to protect environmental and public health. In Malaysia, effluent discharged is regulated under the Environmental Quality Act 1974 (EQA 1974) and Environmental Quality (Sewage) Regulations in 2009, which is governed by the Department of Environment (DOE). The phosphorus limit for domestic effluents in Standard A is 5.0 mg/L, and for other inland waters, Standard B is 10.0 mg/L (DOE, 2009). Compared with other countries, Malaysia's discharge limits are considered less rigorous. However, these limits are relatively higher than international standards. For example, the United States and Japan typically enforce limits below 0.1 mg/L, while the European Union Water Framework Directive applies stricter regulations of 0.05 mg/L in sensitive ecosystems. This comparison highlights the need for more effective phosphorus strategies to meet global water quality expectations and support long-term environmental sustainability.

Various techniques have been used for phosphorus removal, including biological treatment, adsorption, membrane filtration, and chemical precipitation [3]. However, each method has inherent limitations. Chemical precipitation is effective but requires large amounts of chemicals and produces high volumes of sludge, increasing operational and disposal costs. Biological processes, such as Enhanced Biological Phosphorus Removal (EBPR), are more sustainable but may show unstable performance, particularly at low phosphorus concentration. Membrane technologies such as reverse osmosis and ultrafiltration offer high removal efficiency but are often limited by energy consumption and high operational costs. These limitations highlight the need for alternative treatments that are both efficient and cost-effective.

Adsorption has emerged as an effective method for phosphorus removal due to its simplicity, cost-effectiveness, and ability to remove phosphorus at low concentrations. In this study, iron-coated hard clam shells were chosen as the adsorbent due to their high availability and calcium carbonate-rich composition. Surface modification through iron coating enhances the active sites and surface roughness, thereby improving phosphate adsorption efficiency. Shell-based materials, such as eggshells, mussels, and oysters, have been widely studied for phosphate removal due to their high calcium carbonate content, which promotes the formation of stable calcium compounds [4]. Iron modification further enhances adsorption through a ligand exchange mechanism, where phosphate ions (PO_4^{3-}) interact strongly with iron hydroxide surfaces to form Fe-P interactions [5]. Phosphate adsorption is believed to occur through interactions between phosphate ions and iron hydroxide surface groups via ligand-exchange and surface-complexation mechanisms. Compared to previously studied materials such as iron-coated waste mussel shells, hard clam shells have a higher carbonate content (95%-99%), providing more reactive sites for phosphate removal. Previous studies reported high initial adsorption efficiency followed by a decline in performance due to pore blockage and site saturation under continuous operation [6]. Overall, the use of iron-coated hard clam shells provides a sustainable, low-cost adsorbent with potential for continuous-flow phosphate removal applications, supporting their practical use in water treatment systems.

The scalability and practical application of adsorption systems under continuous flow conditions require a clear understanding of adsorbent performance and dynamic behavior. In this study, the efficiency of modified iron-coated hard clam shells for phosphate removal is evaluated using three models: Bed Depth Service Time (BDST), Thomas model, and Modified

Mass Transfer Factor (MMTF). These models are applied to analyze breakthrough behavior, adsorption kinetics, and mass transfer mechanisms in the up-flow column system. Previous studies on shell-based phosphate adsorbents have mainly focused on batch systems or unmodified materials, emphasizing equilibrium removal performance without adequately addressing behavior in continuous-flow systems, thereby limiting their applicability to real-world water treatment processes [7]. In addition, the systematic application and validation of dynamic adsorption models such as Bed Depth Service Time (BDST), Thomas, and Modified Mass Transfer Factor (MMTF) remain limited, particularly in continuous up-flow column systems, which remain insufficiently explored [7]. Therefore, this study aims to investigate phosphate removal performance, adsorption mechanisms, and mass transfer characteristics of modified iron-coated hard clam shells using a model-based approach in a continuous up-flow column system.

Although shell-based adsorbents, such as mussel shell, have shown promising phosphate removal performance [5], their behavior and mass transfer mechanisms under continuous-flow conditions remain insufficiently described. In particular, the combined effect of surface modification and dynamic adsorption behavior in column systems has not been fully explored. This study hypothesizes that iron-coated hard clam shells can enhance phosphate removal efficiency in an upflow column system by increasing surface reactivity and improving mass transfer, while maintaining structural stability during operation. Therefore, this study aims to evaluate the performance of modified iron-coated hard clam shells for phosphate removal under continuous flow conditions. Specifically, the effects of bed depth on removal efficiency and adsorption behavior are investigated, the physicochemical properties of the adsorbent before and after adsorption are examined, and the adsorption process is analyzed using the Bed Depth Service Time (BDST), Thomas, and Modified Mass Transfer Factor (MMTF) models.

2. Materials and Methods

2.1. Synthetic water solution.

Potassium dihydrogen phosphate (KH_2PO_4) of analytical grade was used as the phosphate source. A 100 mg L^{-1} orthophosphate stock solution was prepared by dissolving 0.1433 g KH_2PO_4 into 1 L of deionized water. A 10 mg L^{-1} phosphate solution was subsequently obtained by diluting 100 ppm of the stock solution to 1 L with deionized water, as shown in Equation (1).

$$C_1V_1 = C_2V_2 \quad (1)$$

Where C_1 is 100 mg L^{-1}, C_2 is 10 mg L^{-1}, and V_2 is 1 L. A 1 L volumetric vial was used to transfer the stock solution, which was then diluted to the mark with deionized water. The solution was labeled, stored in a cool, dust-free environment, and gently inverted to ensure a uniform mixture.

2.2. Adsorbent.

Hard clam shells were collected from coastal regions in Kuala Selangor, Malaysia. The raw shells were washed using water to remove impurities, dried, crushed, and sieved to obtain a particle size of 1.18 – 2.36 mm [8]. For surface modification, an alkaline Ferrum (III) solution was prepared by adding Sodium Hydroxide (NaOH) to Ferrum (III) Nitrate $Fe(NO_3)_3$ $9H_2O$

until the pH reached 9.5 ± 0.1. The shell samples were immersed in this solution and agitated for 24 hours at room temperature to promote uniform deposition of iron oxy-hydroxide on the shell surfaces. The samples were then filtered, rinsed, and dried. The modified iron-coated shells were then stored in airtight containers until use in column experiments [9]. The physical and chemical material properties of the modified adsorbent are stated in Table 1.

Table 1. Material properties of the adsorbent material: modified iron-coated hard clam shells.

Composition	Adsorbent form	Particle size	Treated	Analysis
Iron-coated Hard clam shells	Powder	1.18 mm to 2.36 mm	Phosphate synthetic wastewater	BDST model Thomas model MMTF model

The modification parameters were selected based on preliminary trials and previous studies on iron-modified shell-based adsorbents. A Ferrum (III) Nitrate $Fe(NO_3)_3$ $9H_2O$ concentration of 0.5 M was adopted as lower concentrations resulted in insufficient iron deposition, while higher concentrations led to particle agglomeration and uneven coating [10,11]. The pH was maintained at 9.5 ± 0.1 to promote effective hydrolysis of Fe(III) and uniform precipitation of iron hydroxide onto the shell surface. Agitation at 170 rpm for 24 hours was applied to ensure homogeneous mixing and consistent coating formation.

2.3. Experimental device and operational procedure.

An up-flow column reactor was employed with six different bed depths. The laboratory-scale reactor consists of a 50 L water storage tank, a perforated acrylic plate (2 mm hole diameter), silicone tubing, a peristaltic pump, six columns packed with iron-coated hard clam shells adsorbent, and sampling bottles, as illustrated in Figure 1. The adsorbent was packed into six columns at different bed depths of 1, 2, 3, 4, 6, and 8 cm to form uniform beds, with gentle tapping applied to minimize void spaces and prevent channeling. The experiments were conducted at ambient laboratory temperature (25 ± 2°C) under isothermal conditions. The influent was continuously pumped from the storage tank into the bottom of the column using a peristaltic pump to establish an up-flow configuration. An influent flow rate of 0.1933 L h^{-1} was selected based on preliminary optimization and previous studies, as lower flow rates enhance adsorption efficiency, reduce axial dispersion, and increase contact time in iron-coated media [6,7]. The system was operated under laminar conditions (Re < 1), with a consistent hydraulic retention time maintained throughout the experiment [11]. The pressure drop across the column was negligible due to the relatively coarse adsorbent particle size (1.18 – 2.36 mm), which helps maintain bed porosity and reduce clogging [12]. Phosphate concentrations were measured at both the influent and effluent to evaluate column performance. The effluent pH was also monitored to assess its impact on the adsorbent's behavior. Before analysis, samples were filtered to remove suspended solids. The design parameters and operating conditions of the up-flow column reactor system are summarised in Table 2.

Phosphate concentrations were determined using a DR6000 Spectrophotometer. Breakthrough curves were constructed to describe adsorption behavior in the column system. Column performance was analyzed using the Modified Mass Transfer Factor (MMTF), Bed Depth Service Time (BDST), and Thomas models. Key parameters, such as Thomas rate constant, equilibrium adsorption capacity, and mass transfer coefficients, were determined to assess adsorption efficiency and system performance.

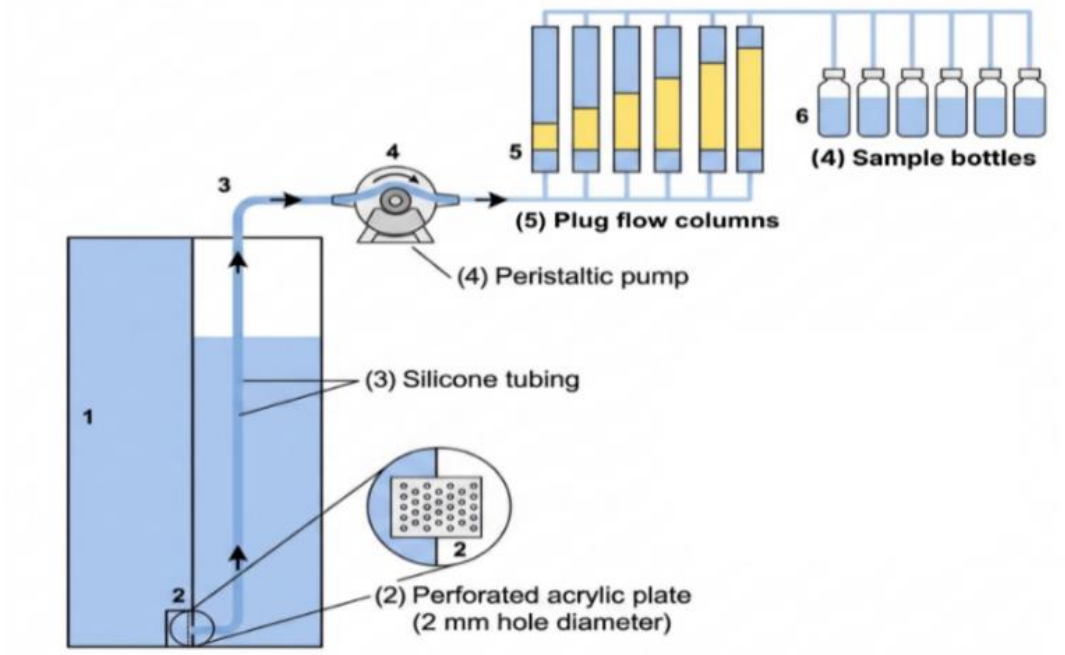

Figure 1. Schematic diagram of the up-flow column reactor illustrating **(1)** water storage tank; **(2)** perforated acrylic plate; **(3)** silicone tubing; **(4)** peristaltic pump; **(5)** plug flow columns; **(6)** sample bottles.

Table 2. Dimensions of plug flow column beds utilized in the up-flow column reactor treatment system.

Parameter	Unit	Dimension
Internal diameter	cm	2.5
Column height	cm	23
Average size of adsorbent	mm	1.18 to 2.36
Volumetric flow rate	L h^{-1}	0.1933
Up-flow column bed depth	cm	1, 2, 3, 4, 6, 8
Amount of adsorbent in the up-flow column	g	8.7749, 15.7164, 23.9548, 31.3505, 48.8137, 61.2983

2.4. Analytical methods.

The modified surface morphology and elemental composition of the adsorbent were analyzed using Scanning Electron Microscopy (SEM) combined with Energy-Dispersive X-Ray Spectroscopy (EDX) and COXEM EM-30 Scanning Electron Microscope. The surface characteristics and interactions between the iron coating and the shell substrate were elucidated by simultaneous SEM-EDX. Fourier Transform Infrared Spectroscopy (FTIR) was conducted using a Perkin-Elmer Spectrometer. X-ray diffraction (XRD) analysis was conducted using the second-generation Bruker D2 Phaser Benchtop Diffractometer. Before the analysis, the samples were cleaned, dried, and finely ground. Phosphate concentrations were measured using a HACH DR6000 Spectrophotometer. Calibration standards between 0 and 5 mg P L^{-1} were generated from analytical-grade KH_2PO_4, and the calibration curve showed excellent linearity, with a correlation coefficient, $R^2 > 0.999$. All samples were analyzed in triplicate, and results are presented as mean ± standard deviation. Blank samples and calibration checks were performed to ensure analytical accuracy and minimize instrumental drift.

2.5. Numerical simulation and data analysis.

2.5.1. Evaluation of up-flow column reactor efficiency.

Phosphate removal efficiency was assessed under various operational conditions, including flow rate, initial phosphate concentration, and bed depth. Breakthrough curves were constructed to describe the variation of effluent phosphate concentration with time, allowing

determination of adsorption capacity, breakthrough time, and exhaustion time. The removal efficiency (*E*) was calculated using Equation (2).

$$E = \frac{(C_{in} - C_{out})}{(C_{in})} \times 100\% \quad (2)$$

Where C_{in} is the initial phosphate concentration at the inlet of the up-flow column reactor (mg L^{-1}), and C_{out} represents the final phosphate concentration at the outlet of the up-flow column reactor (mg L^{-1}).

2.5.2. Bed depth service time (BDST) model.

The BDST model was applied to evaluate the relationship between service time and bed depth in the up-flow column systems. It is useful for predicting column performance and estimating the operational lifespan before breakthrough. The linear form of the BDST equation can be expressed as a linear equation [5], as presented in Equation (3).

$$t = \frac{N_0 \times h}{C_0 \times v} - \frac{1}{K_a \times C_o} \ln\left(\frac{C_o}{C_s} - 1\right) \quad (3)$$

Where *t* is the service time (h), N_o is the dynamic adsorption capacity per unit volume of the up-flow column reactor (mg L^{-1}), C_o is the phosphate concentration entered the up-flow column reactor, *v* is the linear flow rate (cm h^{-1}), K_a is the adsorption rate constant (L h^{-1} mg^{-1}), *h* is the depth of the up-flow column reactor (cm), C_s is the influent phosphate concentration entering the up-flow column reactor (mg L^{-1}). The simplified linear form of the BDST equation is expressed in Equation (4).

$$t = (a\ x\ h) - b \quad (4)$$

Where *t* represents the bed's service time, with $a = N_o/(C_o \text{ x } v)$ is a constant (h cm^{-1}) and *h* is the depth of the up-flow column reactor (cm), and $b = \frac{1}{K_a \times C_o} \ln\left(\frac{C_o}{C_s} - 1\right)$ (h). From the *b* equation, the value of K_a can be written in the form of Equation (5).

$$K_a = \frac{1}{b \times C_o} \ln\left(\frac{C_o}{C_s} - 1\right) \quad (5)$$

Plotting *t* versus *h* yields a straight line, allowing the slope (*a*) and Y-intercept (*b*) to be determined. Once the linear relationship is established, the value of N_o for a given set of C_o and *V* can be calculated. The variation in K_a with respect to the outflow percentage is then determined using Equation (5).

2.5.3. Thomas model.

The Thomas model was used to describe adsorption kinetics and predict breakthrough behavior in the column system. It assumes that adsorption follows Langmuir kinetics under flow conditions. The model equation is given in Equation (6) [6].

$$\frac{C_s}{C_o} = \frac{1}{1 + \exp[K_T\left(\frac{q_o \times m - C_o \times V}{Q}\right)}} \quad (6)$$

Where K_T is the kinetic coefficient or the Thomas rate constant (L h^{-1} mg^{-1}), q_o is the equilibrium phosphate solute uptake per gram of iron-coated hard clam shells adsorbents (mg g^{-1}), and m is the mass of the adsorbent in the up-flow column reactor (g). Q is the volumetric flow rate (L h^{-1}), and V is the effective volume of the synthetic phosphate solution passed through the reactor (L). The terms C_s and C_0 represent the phosphate concentration in the effluent and influent, respectively (mg L^{-1}). By rearranging Equation (6), the Thomas model can be written in the linear form shown in Equation (7) [6].

$$ln\left(\frac{C_o}{C_s}-1\right)=-(c\times t)+d \quad (7)$$

Where $c = K_T$ x C_0 as the slope is a constant (h^{-1}), $t = V/Q$ is the service time (h), and $d = \frac{K_T\times q_o\times m}{Q}$. Since the y-intercept is a constant (dimensionless), the experiment was set at a constant flow rate. Since the values of a slope and d as the Y-intercept have been confirmed from the linear curve, $\left[ln\left(\frac{C_o}{C_s}-1\right)\right]$ in versus t allows us to compute the value and the value at a certain flow rate [13].

2.5.4. Modified mass transfer factor (MMTF) model.

The MMTF model was applied to calculate the cumulative amount of phosphate adsorbed onto the adsorbent over time. The cumulative amount of phosphate deposited on the modified iron-coated hard clam shells' surface can be determined using Equation (8) [6].

$$q=\int_0^V\frac{(C_o-C_s)dV}{m} \quad (8)$$

Where q is the cumulative quantity of phosphate deposited on the modified iron-coated hard clam shells surface at a volume of V of synthetic phosphate solution flowing through the up-flow column reactor bed (mg g^{-1}). The adsorbate concentration at any given time and position in the column can be predicted using the standard Equation (8), which can be written as Equation (9).

$$\ln\left(\frac{C_o}{C_s}\right)=[k_La]_g\times e^{-\beta\times\ln(q)}\times t \quad (9)$$

Where $[k_La]_g$ is the global mass transfer factor (h^{-1}) and β is the adsorbate-adsorbent affinity parameter (g h mg^{-1}). The simplification of Equation (9) resulted in a linear equation that can be written as Equation (10).

$$\ln(q)=\frac{1}{\beta}\times\ln(t)+B \quad (10)$$

With:

$$B=\frac{\ln([k_La]_g)-\ln\left\{ln\left(\frac{C_o}{C_s}\right)\right\}}{\beta} \quad (11)$$

Where B is the potential mass transfer index linked to the driving force of phosphate mass transfer from bulk water to acceptor sites (mg g^{-1}). The external mass transfer factor's correlation $\left([k_La]_f\right)$ and $[k_La]_g$ can be expressed in the form [6] of Equation (12).

$$[k_L a]_f = [k_L a]_g \times e^{-\beta \times \ln(q)} \quad (12)$$

Where $[k_L a]_f$ is the external (film) mass transfer factor (h^{-1}). By plotting $\ln(q)$ versus $\ln(t)$, allow us to verify the values of β from the slope and B from the y-intercept of the straight line. The parameters β and B are empirical constants obtained from model fitting and are used to describe adsorption trends. The value $[k_L a]_g$ minus $[k_L a]_f$ is the value of internal mass transfer $[k_L a]_d$, which can be expressed in Equation (13) [5].

$$[k_L a]_d = [k_L a]_g - [k_L a]_f \quad (13)$$

Where $[k_L a]_d$ is the internal mass transfer factor (porous diffusion) factor (h^{-1}). Equation (10), which describes the transport mechanism of phosphate moved through the matrix pores, can be used to verify the variation $[k_L a]_d$ value followed by the values of $[k_L a]_g$ and $[k_L a]_f$. It can also be used to determine mass transfer resistance by comparing the variation pattern of $[k_L a]_d$ with $[k_L a]_f$ for the adsorption of phosphate from contaminated water onto the iron-coated hard clam shells adsorbent.

The BDST, Thomas, and modified mass transfer factor (MMTF) models applied in this study provide complementary insights into the adsorption process. The BDST model describes the relationship between bed depth and service time, enabling the prediction of column lifespan. The Thomas model evaluates adsorption kinetics and capacity based on breakthrough behavior, while the MMTF model offers a detailed analysis of mass transfer mechanisms, including external film and internal pore diffusion. These models enable a comprehensive assessment of adsorption performance under continuous flow conditions. The adsorption behavior predicted by these models is supported by the structural and chemical changes observed in the characterization analyses. Non-linear regression analysis was performed using Microsoft Excel. Model parameters were obtained by fitting the experimental data to the respective model equations. The summary of the experimental workflow for phosphorus adsorption using modified iron-coated hard clam shells in an up-flow column system is shown in Figure 2.

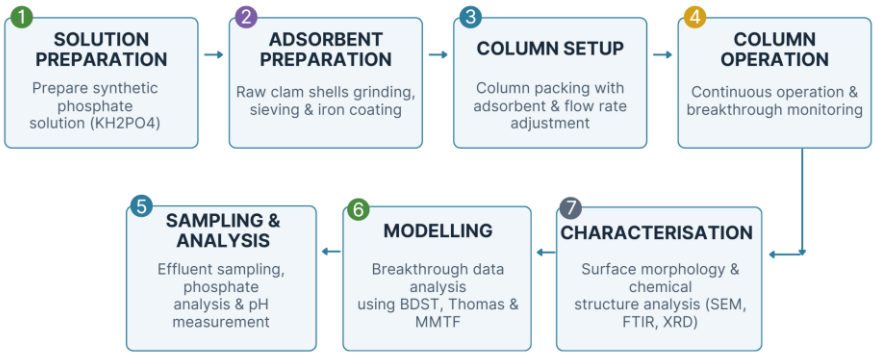

Figure 2. Experimental workflow for phosphorus adsorption using modified iron-coated hard clam shells in an up-flow column system.

3. Results and Discussion

3.1. Physical and chemical characteristics.

The FTIR spectrum of iron-coated hard clam shells provides information on the functional groups present before and after phosphate adsorption. Based on Figure 3, a

prominent band was observed at approximately 1471 - 1490 cm^{-1}, corresponding to the stretching vibration of carbonate (CO_3^{2-}), which is the main component of the shell structure ($CaCO_3$). After phosphate adsorption, a band appeared at around 859 cm^{-1}, which can be attributed to P–O vibrations, indicating the presence of phosphate-related functional groups. This suggests that phosphate ions interacted with the modified surface, likely through bonding with the iron-coated layer. These changes in the FTIR spectrum confirm that surface modification enhanced the chemical interaction between phosphate ions and the adsorbent [6].

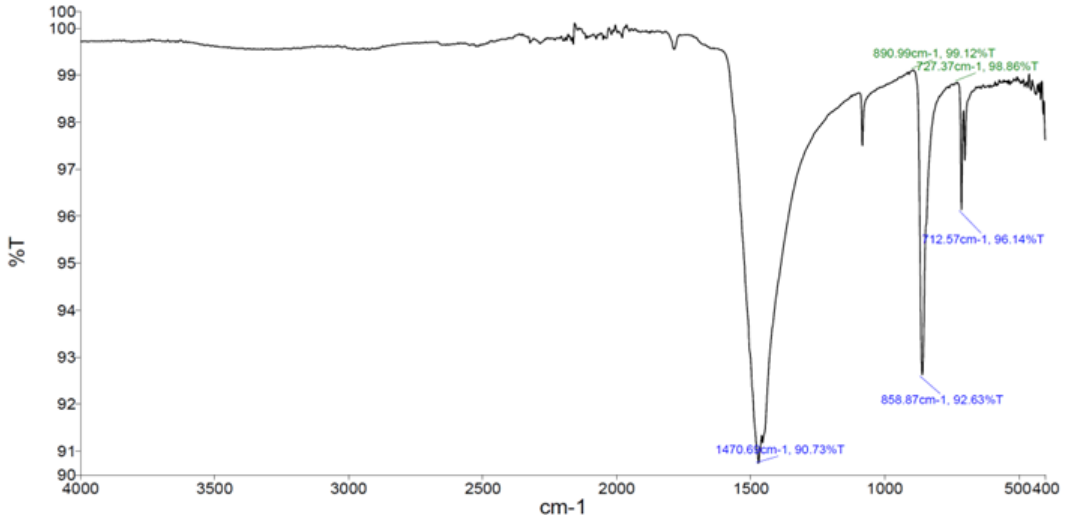

Figure 3. FTIR spectrum after the adsorption of phosphate.

The functional group assignments corresponding to the adsorption bands identified in the FTIR spectrum are summarized in Table 3.

Table 3. FTIR functional group assignments for adsorption bands.

Adsorption (cm^{-1})	Detection of functional group	
1471	Bidentate carbonate	
891	Bidentate carbonate	
859	Aromatic phosphates, P-O-C stretch	
713	Aromatic phosphates, P-O-C stretch	

The XRD patterns of the iron-coated hard clam shells before and after phosphate adsorption are shown in Figure 4. Before adsorption, the diffraction peaks correspond predominantly to aragonite, confirming that calcium carbonate ($CaCO_3$) is the main crystalline phase of the shell material. Its presence increases the shell's mechanical strength and resilience, increasing its resistance to external stress and breakdown [10]. After adsorption, the XRD pattern shows that the dominant aragonite structure is preserved, with no significant shift in peak positions. This indicates that the adsorption process does not alter the shell's bulk crystalline structure. However, slight variations in peak intensity and the appearance of minor additional peaks were observed, which may be attributed to surface interactions between phosphate ions and the modified shell surface. This phase change may be attributed to structural rearrangement during adsorption and interaction with the iron coating [11]. The absence of distinct crystalline iron or phosphate phases suggests that adsorption occurs mainly at the surface level rather than through bulk structural transformation. These results confirm that the modified iron-coated hard clam shells maintain structural stability while providing active sites for effective phosphate adsorption.

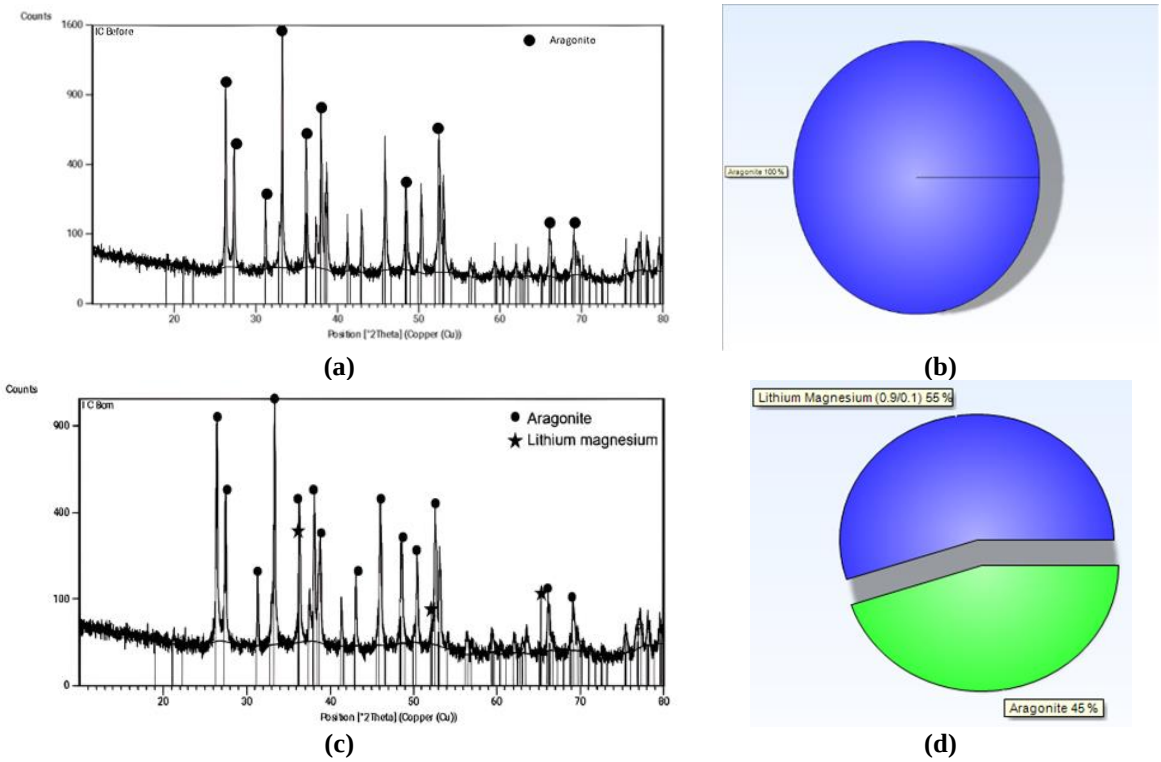

Figure 4. (a) XRD before adsorption pattern; **(b)** Before adsorption pie chart; **(c)** XRD after adsorption pattern; **(d)** After adsorption pie chart of modified iron-coated hard clam shells.

The EDXRF results in Table 4 show that calcium (Ca) and oxygen (O) were the dominant elements in the iron-coated hard clam shell, confirming that calcium carbonate ($CaCO_3$) is the main structural component of the adsorbent. The Ca content increased slightly from 29.70% before adsorption to 31.53% after adsorption, while O increased from 53.04% to 65.51%. This may be associated with surface interaction and the formation of oxygen-containing phosphate complexes after adsorption. The presence of Fe before adsorption (0.46%) indicates that iron was successfully introduced onto the shell surface during the modification process [14]. After adsorption, Fe was not detected by EDXRF, suggesting that the detectable iron signal was reduced after phosphate uptake. This may be due to the involvement of iron species in phosphate binding or the coverage of iron-active sites by adsorbed phosphate species. Minor elements such as Na, Mg, Al, and Sr were also detected in small amounts. These elements are commonly associated with the natural shell composition and may contribute to the adsorbent's mineral structure. Although the shell does not normally contain CaO, it can be produced by thermal decomposition, or calcination, in which heating calcium carbonate produces CO_2 and CaO [15].

Table 4. Chemical composition of iron-coated hard clam shell (%) analyzed by EDXRF spectrometer.

Element	Weight before adsorption (%)	Weight after adsorption (%)
Ca	29.70	31.53
O	53.04	65.51
Na	0.14	0.59
Mg	0.01	0.19
Al	0.39	0.27
Sr	0.11	0.35
Fe	0.46	0.00

A scanning electron microscope (SEM) is a microscope that provides high-magnification images of samples to determine a material's surface topography, composition, and structure. A focused electron beam is scanned over a sample's surface, generating signals

that provide detailed information on the sample's composition, surface characteristics, and other attributes [16]. The surface morphology of the iron-coated hard clam shells was examined using SEM at 2000x magnification, as shown in Figure 5. Before adsorption, the surface appeared rough and irregular, with relatively compact features. After adsorption, the surface became more heterogeneous, with the presence of granular deposits and increased surface texture. These changes indicate the formation of a coating layer and the accumulation of adsorbed phosphate species on the shell surface. The development of a more porous, irregular structure after modification increases the available surface area and provides more active sites for phosphate adsorption. These observations are consistent with improved adsorption performance of the modified material.

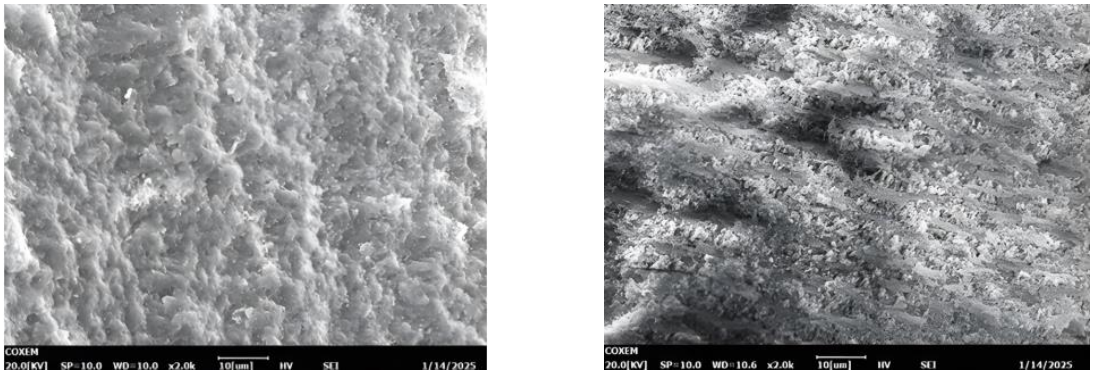

(a) **(b)**

Figure 5. SEM image of iron-coated hard clam shells at 2000x magnification **(a)** before; **(b)** after adsorption.

The combined SEM–EDX, FTIR, and XRD analyses provide consistent evidence supporting the successful modification of the hard clam shells. SEM–EDX observations confirm the presence and distribution of iron on the adsorbent surface, while FTIR spectra show enhanced Fe–O and P–O bands, indicating interaction between phosphate ions and the modified surface. XRD results demonstrate that the dominant crystalline structure is largely preserved, with only minor changes after adsorption, suggesting that the process occurs mainly at the surface. These findings indicate that surface modification enhances the adsorbent's reactivity by introducing additional active sites and improving its surface characteristics. The rougher morphology and more uniform iron distribution observed in SEM images promote improved contact between phosphate ions and the adsorbent. At the same time, the presence of iron-related functional groups supports adsorption through surface complexation mechanisms. This improved physicochemical behavior is consistent with the column performance, including increased adsorption capacity and extended service time as predicted by the Thomas and BDST models, as well as enhanced mass transfer characteristics described by the MMTF model. The absence of detectable Fe after adsorption may be attributed to surface coverage by phosphate species or limitations in detection sensitivity, rather than complete removal of iron. Overall, these findings demonstrate a clear relationship between surface modification and improved phosphate removal performance under continuous flow conditions.

3.2. Performance of the up-flow column reactor.

The findings in Figure 6(a) demonstrate that the up-flow column reactor reached a maximum removal efficiency 65.1% (8 cm), 56.3% (6 cm), 43.2% (4 cm), 42.9% (3 cm), 33.1% (2 cm), and 24.8% (1 cm). An increase in the pore space and acceptor sites of the modified iron-coated hard clam shells adsorbent occupied by the various solutes may be the cause of a decline in the up-flow column reactor performance, which may be tracked by a rise in solute

breakthrough during the experiment. After 24 hours of the experiment, the removal efficiency of phosphate was observed to have decreased by 2.7% from 65.1% to 62.4% (8 cm). This could be because the positively charged Ca^{2+} and Fe^{2+} ions on the surface of modified iron-coated hard clam shells aid in the adsorption of negatively charged phosphate ions from the water effluent. The reactive surface of CaO, Fe_2O_3, and $CaCO_3$ occupied by the phosphate ions, then rapidly declines during 144 hours from 24 to 168 hours of the experiment, which may be the reason why the up-flow column reactor performance dropped by 16.8% from 62.4% to 45.6% (see 8 cm). The rapid increase in removal efficiency with increasing contact length illustrates how quickly the adsorbate occupied the adsorbent's empty sites until equilibrium was reached, when all the sites were fully occupied [12]. In comparison, previous studies on iron-coated waste mussel shell (ICWMS) in batch systems reported significantly higher phosphate removal efficiencies of 95.7%–96.9% with an adsorption capacity of approximately 0.30 mg g^{-1} under extended contact times (48–120 hours) [7,17]. However, these values were obtained under equilibrium batch conditions and do not reflect continuous-flow behavior. The present study demonstrates lower, but more practically relevant, performance under dynamic upflow conditions, which better represent real wastewater treatment operations.

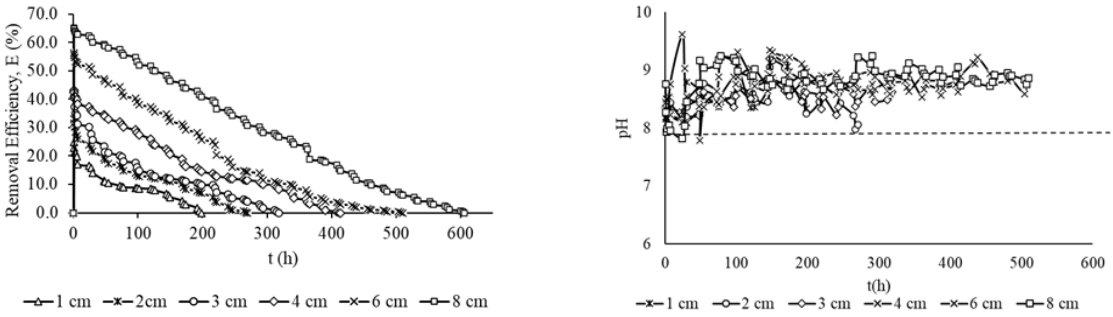

(a) **(b)**

Figure 6. (a) Removal efficiency of water effluent phosphate; **(b)** pH performance of water effluent in the up-flow column reactor.

The trends observed in Figure 6 can be explained by the interaction between the modified surface chemistry and the hydrodynamic behavior of the up-flow column. The higher removal efficiencies at greater bed depths are attributed to the increased number of active sites provided by thicker layers of modified iron-coated shells, which enhance both the initial adsorption rate and the contact time between phosphate ions and the reactive surfaces. As the bed depth increases, diffusion resistance decreases relative to the number of available adsorption pathways, resulting in delayed breakthrough and improved overall removal. The gradual decline in performance during prolonged operation is primarily due to progressive saturation of Fe–OH and Ca–OH binding sites, consistent with phosphate-displacement and precipitation pathways reported in previous studies [6]. The variations in pH shown in Figure 5(b) also correlate with ion-exchange processes and Fe-oxide buffering effects, where OH^- consumption during Fe–P complexation results in slight pH reductions at higher adsorption intensities. These mechanistic explanations provide a clearer cause–and–effect understanding of the observed patterns and strengthen the interpretation of column performance.

In addition to recording the phosphate removal efficiency, the pH of the water effluent has also been recorded, as shown in Figure 5(b). Depending on the species and kind of water body, an aquatic ecosystem's ideal pH range is typically between 6.5 and 8.5. While some fish and aquatic plants can withstand slightly more acidic or alkaline conditions, freshwater ecosystems such as rivers, lakes, and ponds generally flourish in a pH range of 6.5 to 8.0. Since

saltwater is inherently somewhat alkaline due to dissolved bicarbonates and carbonates, marine habitats, such as oceans and estuaries, typically have a pH of 8.0 to 8.3. The average blood pH of fish and other vertebrates is 7.4. For farmed fish, a pH range of 6.5 to 9.0 is advised. The alkaline death point is approximately 11, and the acid death point is approximately 4 [18]. During the 24-hour experiment, the pH fluctuations were recorded at the storage tank. They ranged from 7.82 to 8.76 with an average of 8.11 (8 cm), pH value of 8.06 to 9.62 with an average of 8.45 (6 cm), pH value of 8.11 to 8.54 with an average of 8.38 (4 cm), pH value of 8.14 to 8.55 with an average of 8.38 (3 cm), pH value of 8.15 to 8.51 with an average of 8.43 (2 cm), and pH value of 8.29 to 8.5 with an average of 8.43 (1 cm). The results show that a higher bed depth of modified iron-coated hard clam shells in the column reactor yields a more neutral pH in the water effluent.

The pH of treated synthetic water may drop as a result of the presence of Iron (III) Oxide in the form of a heterolytically dissociated structure on the surface of modified iron-coated hard clam shell, which may draw OH-ions from solution attached to the surface site of Fe^{3+} ions. Similarly, the study using iron-coated waste mussel shells reported a gradual decrease in effluent pH, attributed to the same Iron (III) Oxide-driven mechanism. However, the decline was more pronounced in the iron-coated waste mussel shells system, possibly due to its lower buffering capacity from reduced calcium carbonate content. This comparison shows that the modified iron-coated hard clam shell provides superior pH stability during phosphate removal, especially at greater bottom depths [6]. One major reason for relatively high or alkaline water pH values is that, depending on water composition and external factors, various chemical and environmental conditions can raise the pH of synthetic water. Frequently, alkaline agents capable of increasing the alkalinity of the solution, such as NaOH, are employed to regulate the pH during the preparation of the modified iron-coated hard clam shell [19].

In comparison to unmodified raw shells, the modified iron-coated hard clam shells demonstrated a substantial increase in phosphate removal. Under comparable conditions, previous studies have indicated that raw hard clam shells typically only remove 18–28% of phosphate [5,11]. By contrast, the modified shells in the present study achieved a removal efficiency of 65.1%, which is equivalent to an improvement of approximately 140 – 260%. This improved performance is corroborated by the FTIR results, which showed enhanced P–O stretching bands, suggesting improved Fe–P interactions in the modification [9].

XRD analysis revealed the formation of new iron hydroxide phases, associated with increased surface reactivity and improved adsorption behavior [6]. SEM–EDX confirmed uniform Fe deposition and more developed pore structures, which increased active surface sites for adsorption. These quantitative and qualitative improvements clearly demonstrate that iron modification significantly enhances the adsorption capability of hard clam shells. This improvement is also notable when compared to iron-coated waste mussel shells reported in previous batch studies, which achieved similar adsorption capacities (~0.30 mg g^{-1}) only under prolonged equilibrium conditions [7,17], where the present study achieves significant removal under continuous flow conditions with shorter contact times. In addition to adsorption performance, the potential for regeneration and reuse of the modified iron-coated hard clam shells is an important consideration for sustainable application. Although regeneration was not experimentally investigated in this study, previous studies on iron-based and calcium-rich adsorbents have shown that phosphate-saturated materials can be partially regenerated through chemical desorption methods, such as alkaline or acid washing. However, repeated regeneration cycles may lead to a gradual decline in adsorption efficiency due to structural

degradation of calcium carbonate and possible loss of active Fe–OH binding sites. In this study, the observed decrease in removal efficiency over prolonged operation suggests progressive saturation of active sites, suggesting that regeneration would be necessary for extended use. Therefore, further investigation on regeneration efficiency, reusability, and long-term stability is required to evaluate the practical feasibility of this adsorbent in continuous water treatment systems.

3.3. Numerical analysis using the bed depth service time (BDST).

The BDST model showed a linear relationship between bed depth and service time, indicating stable adsorption performance under different operating conditions. Higher bed depth resulted in longer service time, confirming that increased adsorbent mass enhances phosphate removal capacity [8]. This trend is observed in the experimental data. From Figure 7, at a bed depth of 1 cm, the column achieved a service time of only 4.71 hours before reaching 91% breakthrough. In contrast, increasing the bed depth to 2 cm significantly extended the service time to 42.75 hours. This substantial increase demonstrates that a greater amount of adsorbent provides more active sites for phosphate adsorption and prolongs the column's operational lifespan. The increase in service time with increasing bed depth can be attributed to improved contact between phosphate ions and the adsorbent surface, as well as reduced mass-transfer limitations. A deeper bed allows more interaction time and enhances the probability of adsorption before breakthrough occurs [20]. The negative K_a values observed are associated with the slope of the linearised BDST equation and do not represent physically negative adsorption rates. The BDST results confirm that bed depth is a key design parameter in the up-flow column system. Increasing bed depth improves adsorption performance, delays breakthrough, and enhances the practical applicability of the modified iron-coated hard clam shells for continuous phosphate removal. This finding is consistent with fixed-bed adsorption theory, where increased bed depth provides a larger adsorption zone and delays saturation.

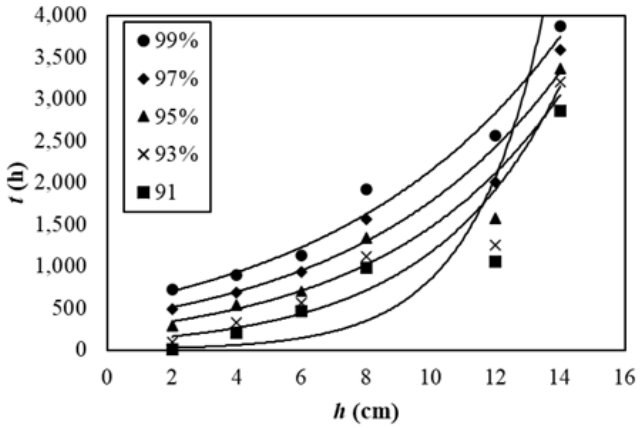

Figure 7. BDST curve of plotting t versus h.

Next, to fill the acceptor sites of CaO, Iron (III) Oxide, and calcium carbonate polymorphs, an increase in the value of N_o corresponding to an increase in the amount of phosphate deposited on the surface of modified iron-coated hard clam shells might not be sufficient. Moreover, as the C_s/C_o ratio rises, the dynamic phosphate adsorption capacity increases. This could be because the water effluent flow increased velocity, resulting in a higher force of phosphate deposition per unit area of the modified iron-coated hard clam-shell adsorbent. Since the dispersion of phosphate caused by the resistance of mass transfer

controlled by either film zone surrounding the solid of modified iron-coated hard clam shells material of phosphate inside the pores of modified iron-coated hard clam shells adsorbent is still negligible, the physical meaning of the constant K_a cannot be clearly understood. This is because an irregular trend of the K_a variation with the increase in the C_s/C_o ratio appeared (Table 5).

Table 5. The parameters N_o and K_a are calculated using the BDST models.

C_S / C_O (%)	a (h cm^{-1})	b (dimensionless)	N_0 (mg L^{-1})	K_a (L h^{-1} mg^{-1})	R^2
80	9.1282	0.5292	3594.10530	-0.26	0.8730
85	32.083	0.3492	12632.2473	-0.50	0.9329
90	81.667	0.2414	32155.2766	-0.91	0.8713
95	151.90	0.1625	59808.5703	-1.84	0.9556
99	184.00	0.1537	72447.5111	-3.00	0.9604

3.4. Numerical analysis using the Thomas model.

The Thomas model can be used to forecast breakthrough curves and to explain the kinetic behavior of phosphate adsorption onto modified iron-coated hard clam shells in the up-flow column reactor. By validating the modified shells' efficacy in removing phosphate, these computations will offer a solid foundation for comprehending the adsorption process's kinetics [21]. The analysis of data obtained from experiments conducted at a flow rate of 0.1933 L h^{-1} for the different depths of the up-flow column reactor bed using the Thomas models can be used to conduct the kinetic research of phosphate adsorption onto the modified iron-coated hard clam shells adsorbent. The values of K_T and q_o can be determined by plotting ln [(C_o/C_s) – 1] versus t using Equation (7), which produces a linear regression slope with the slope denoted as c and the Y-intercept as d that progressively increases with increasing h, as shown in Figure 8.

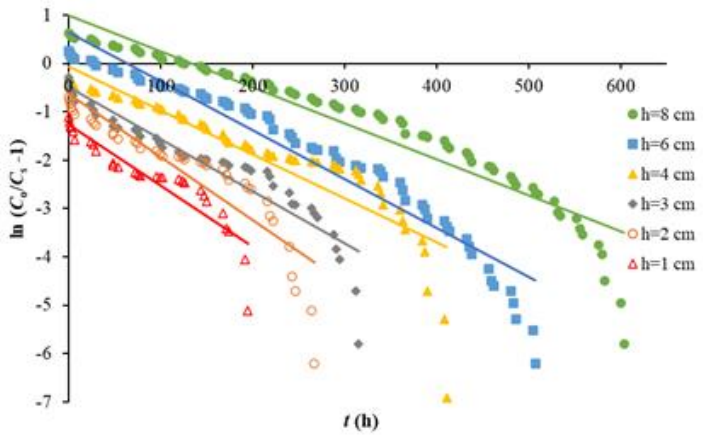

Figure 8. A plot of *ln* [(C_o/C_s) – 1] versus t for the adsorption of phosphate at six different depths of the iron-coated hard clam shell.

The kinetic behaviors of phosphate that traveled from water effluent to the surface of modified iron-coated hard clam shells may be described by using the K_T and q_o values because of the correlation for the parameters (R^2 > 0.845; see Table 6). The numerical analysis using the Thomas Model reveals a clear trend in the adsorption behavior of phosphate as a function of bed depth in the up-flow column reactor. As the bed depth increased progressively from 1 cm, 2 cm, 3 cm, 4 cm, 6 cm, and 8 cm, the Thomas rate constant (K_T) fluctuated slightly but showed a general declining trend: starting at 0.0013 L h^{-1} mg^{-1} for both 1 cm and 2 cm depths, dropping to 0.0011 L h^{-1} mg^{-1} at 3 cm, further to 0.0009 L h^{-1} mg^{-1} at 4 cm, slightly increasing to 0.0010 L h^{-1} mg^{-1} at 6 cm, and finally declining again to 0.0007 L h^{-1} mg^{-1} at 8 cm. This

variation suggests that as bed depth increases, the rate of phosphate adsorption slows due to extended contact time and deeper diffusion zones. Negative Thomas parameters observed at lower bed depths were interpreted cautiously, as they may reflect limitations of the model fitting under early breakthrough conditions. Similar observations have been reported in fixed-bed adsorption studies, where Thomas model parameters are influenced by the regression approach, fitting region, and non-ideal breakthrough behavior. Therefore, these values do not represent physically negative adsorption behavior but indicate reduced model applicability under certain operating conditions [22]. Simultaneously, the maximum adsorption capacity (q_o) showed a steady improvement, from a negative value of -22.03 mg g^{-1} at 1 cm, gradually increasing through -5.95 mg g^{-1} and -3.69 mg g^{-1} at 2 and 3 cm respectively, turning positive at 4 cm (-0.4 mg g^{-1}), and further increasing to 2.49 mg g^{-1} at 6 cm and 4.21 mg g^{-1} at 8 cm. (see Table 6). This suggests that deeper beds support more effective phosphate uptake per gram of adsorbent, likely due to increased contact surface and retention time.

A significant amount of phosphate deposited on the surface of modified iron-coated hard clam shells material can be retained because the dispersion of phosphate ions throughout the modified iron-coated hard clam shells adsorbent can be enlarged with an increase in modified iron-coated hard clam shells in the up-flow column reactor bed. Because the pore space feature of modified iron-coated hard clam shells is sensitive to the internal structure and chemical functional groups of the acceptor sites, the kinetic coefficient, K_T decreased when the water velocity dropped due to an increase in the modified iron-coated hard clam shells dosage. The external mass transfer of phosphate from the bulk liquid to the solid surface of the modified iron-coated hard clam shell adsorbent is associated with the application of Thomas models for phosphate adsorption, which may aid in explaining the collision frequency and driving force of the mass transfer. Compared to the previous study using iron-coated waste mussel shells, a similar decline in K_t values was observed with increasing bed depth. However, the iron-coated waste mussel shell system showed a significantly higher initial adsorption efficiency but experienced a more rapid decline in performance over time, as reflected in its K_t and q_o values. In contrast, the modified iron-coated hard clam shells exhibit a consistent increase in adsorption capacity (q_o) with increasing bed depth, suggesting that their long-term adsorption potential is improved. The modified shells' enhanced performance, particularly their ability to sustain phosphate removal efficacy during extended column operation, is demonstrated by this behavior [6].

Table 6. Thomas model parameters, K_T and q_o.

***h* (cm)**	***m* (mg)**	**K_T (L h^{-1} mg^{-1})**	**q_o (mg g^{-1})**	**R^2**
1	8.8	0.0013	-22.03	0.845
2	15.7	0.0013	-5.95	0.811
3	24.0	0.0011	-3.69	0.876
4	31.4	0.0009	-0.4	0.807
6	48.8	0.0010	2.49	0.930
8	61.3	0.0007	4.21	0.908

The structural and chemical changes identified through physicochemical characterization confirmed the adsorption patterns predicted by the BDST, Thomas, and MMTF models, indicating a coherent mechanism governing phosphate removal in the up-flow column system. The BDST model demonstrates that increasing bed depth prolongs service time, confirming that greater adsorbent mass enhances adsorption capacity. Similarly, the Thomas model shows an increase in adsorption capacity (q_o) with bed depth, although accompanied by a decrease in the rate constant (K_T), suggesting the presence of diffusion

limitations at higher bed depths. This trend is further supported by the MMTF model, which indicates improved overall mass transfer performance alongside reduced internal diffusion resistance. These findings suggest that phosphate adsorption is controlled by a combination of surface interaction and mass transfer processes. The increase in adsorption capacity and service time reflects the availability of more active sites and longer contact time, while the reduction in apparent kinetic rates highlights the influence of transport limitations within the column. The results indicate that the agreement among the three models suggests that the modified iron-coated hard clam shells exhibit stable, efficient adsorption performance under continuous-flow conditions. This integrated modeling approach provides a more reliable basis for scaling up the adsorption system for real wastewater applications.

3.5. Numerical analysis using the modified mass transfer factor model.

A linear relationship between ln(q) versus ln(t) according to Equation (9) was shown in Figure 9 at different bed depths (1 – 8 cm). The slope of the regression line increased with bed depth, suggesting changes in the interaction between phosphate ions and the adsorbent surface. This may indicate that adsorption is more influenced by diffusion processes at greater bed depths, where longer contact times and deeper packing affect mass-transfer behavior. In addition, the y-intercept (B) shifted towards more negative values with increasing bed depth, indicating a reduction in the apparent driving force for phosphate transport from the bulk solution to the adsorbent surface. This trend suggests that mass transfer resistance increases with bed depth, likely due to partial saturation of active sites and increased diffusion pathways within the packed bed. Despite this, the overall adsorption performance remained effective, as supported by the BDST and Thomas model results, which showed improved service time and adsorption capacity at higher bed depths.

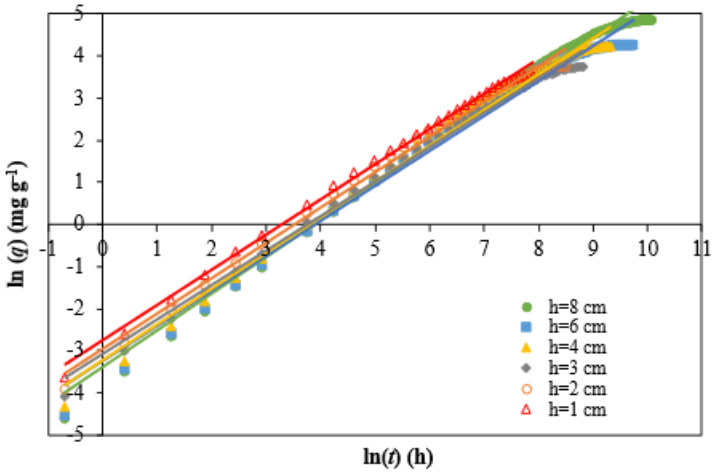

Figure 9. Linear regression of ln(q) versus ln(t) for the PO_4^{3-} adsorption onto iron-coated hard clam shells.

The variation in $[k_La]_g$, $[k_La]_f$, and $[k_La]_d$ indicates that mass transfer behavior changed with bed depth, reflecting differences in contact time, available active sites, and diffusion pathways. Higher bed depths generally improved phosphate transport and adsorption performance by increasing interaction between the phosphate ions and the modified shell surface. These findings support the BDST and Thomas model results, which showed longer service time and higher adsorption capacity at greater bed depths. The MMTF analysis suggests that phosphate removal by modified iron-coated hard clam shells is governed by the combined effects of surface adsorption and mass transfer resistance [23].

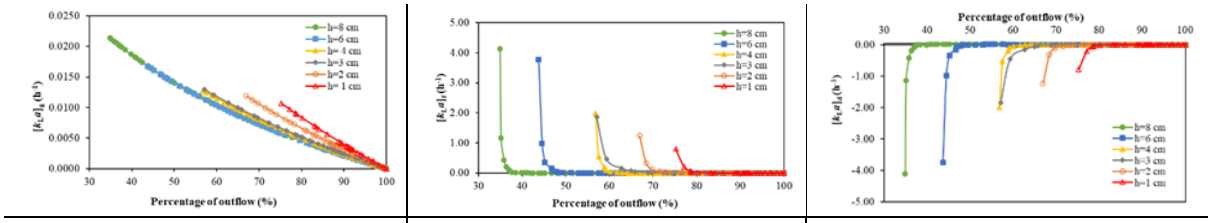

(a) **(b)** **(c)**

Figure 10. MMTF curve of plotting parameters; **(a)** $[k_La]_g$; **(b)** $[k_La]_f$; **(c)** $[k_La]_d$ with percentage of outflow (%).

The variation of the global mass transfer coefficient $[k_La]_g$ with effluent outflow percentage at different bed depths is presented in Figure 10(a). The results show that $[k_La]_g$ gradually decreases as the outflow percentage increases, indicating a reduction in mass transfer rate during continuous operation. This behavior is expected as adsorption sites become progressively occupied over time. Higher bed depths (6 cm and 8 cm) consistently exhibited higher [kLa]g values than shallower beds, suggesting improved mass transfer performance due to increased contact time and greater availability of active sites. In contrast, shallower beds (1 cm and 2 cm) showed a more rapid decline in $[k_La]_g$, indicating earlier saturation and reduced adsorption efficiency.

Figure 10(b) illustrates the variation of the external film mass transfer coefficient $[k_La]_f$. Deeper beds showed higher initial $[k_La]_f$ values, particularly at lower outflow percentages, indicating stronger initial mass transfer from the bulk solution to the adsorbent surface. As the bed depth decreased, the peak values shifted towards higher outflow percentages, suggesting delayed and less efficient external mass transfer [24]. However, at greater depths, the adsorption rate decreases rapidly due to the saturation of active sites, confirming that adsorption kinetics depend on the bed depth and the available surface area of the modified iron-coated hard clam shell adsorbent [25].

The desorption mass transfer coefficient $[k_La]_d$, shown in Figure 10(c), followed a similar trend. Higher values were observed at a bed depth of 8 cm, reaching approximately 4.2 h^{-1} at around 35% outflow, indicating enhanced diffusion of phosphate ions into the adsorbent's internal pore structure. In contrast, lower bed depths, 2 cm and 1 cm, exhibit the lowest $[k_La]_d$ values, with maximum coefficients of approximately 1.5 h-1 and 1.0 h^{-1} occurring at higher outflow percentage (70% to 75%), exhibited reduced $[k_La]_d$ values, suggesting limited internal diffusion and faster saturation of adsorption sites.

Overall, the results indicate that increasing bed depth enhances both external and internal mass transfer processes, leading to improved phosphate removal performance [6]. However, the gradual decline in mass transfer coefficients with increasing outflow percentage reflects the influence of adsorption site saturation and diffusion limitations during prolonged operation. The β parameter remained relatively constant, from 1.150 to 1.224 g h mg^{-1} across all bed depths, indicating stable overall mass transfer behavior throughout the column operation, as shown in Table 7. It demonstrated a downward trend as the bed depth increased, with the highest value recorded at 8 cm (-3.388 mg g^{-1}). This pattern indicates that increased adsorbent loadings facilitate greater phosphate uptake. The high correlation coefficients (R^2 = 0.980–0.996) indicate that the MMTF model adequately describes the adsorption behavior under the investigated conditions. It is crucial to optimize column height to balance phosphate removal efficiency and adsorbent regeneration [26]. These findings demonstrate that phosphate adsorption in the up-flow column system is governed by a combination of film diffusion and pore diffusion mechanisms, with bed depth playing a critical role in controlling mass transfer

efficiency and overall system performance. However, a direct quantitative relationship between structural features and mass transfer coefficients was not established in this study.

Table 7. Parameter β and B value at different depths of the up-flow column.

h (cm)	β (g h mg^{-1})	B (mg g^{-1})	R^2
1	1.198	-2.742	0.996
2	1.194	-2.949	0.993
3	1.224	-3.078	0.993
4	1.168	-3.244	0.991
6	1.203	-3.241	0.980
8	1.150	-3.388	0.987

Compared to earlier studies that used raw or iron-modified shell-based adsorbents, the modified iron-coated hard clam shells evaluated in this study showed more stable and improved phosphate removal performance. Previous work on iron-coated waste mussel shells reported high initial adsorption by a rapid decline, mainly due to pore saturation and the lower calcium carbonate content of the material [9]. In contrast, the modified hard clam shells in the study maintained longer breakthrough times and exhibited higher adsorption capacities as bed depth increased. This improved performance is related to the naturally higher $CaCO_3$ content (95 – 99%) and more uniform iron distribution on the shell surface. In addition, while many earlier studies focused mainly on batch adsorption kinetics, this study extends existing knowledge by incorporating continuous-flow column modeling using the BDST, Thomas, and MMTF models supported by comprehensive physicochemical characterization (FTIR, XRD, SEM-EDX). This combination of experimental investigation and modeling provides a clearer understanding of the adsorption mechanism and mass transfer behavior under practical operating conditions. The results indicate that modified iron-coated hard clam shells can serve as a sustainable and promising adsorbent for phosphate removal in continuous-flow systems.

4. Conclusions

This study used modified iron-coated hard clam shell materials as an alternative sustainable adsorbent to remove phosphate in an up-flow column reactor. A maximum removal efficiency of 65.1% was achieved at a bed depth of 8 cm, indicating that adsorption performance improves with increased adsorbent mass and contact time. The data analysis using the BDST, Thomas, and modified mass transfer factor (MMTF) models showed reasonable agreement with the experimental data (R^2 = 0.84–0.99), indicating that these models can adequately describe adsorption behavior under continuous flow conditions. The results indicate that adsorption capacity and service time increase with bed depth, whereas mass-transfer limitations become more significant at greater depths due to diffusion resistance. Physicochemical characterization further supports these findings, indicating that surface modification increases the number of active sites and improves adsorption performance. Although the removal efficiency is moderate, the use of waste-derived hard clam shells provides a low-cost, environmentally friendly alternative for phosphate removal. The results suggest that modified iron-coated hard clam shells have potential for phosphate removal under continuous-flow conditions and may be applicable to real wastewater treatment. Future research should focus on pilot-scale studies using real wastewater, as well as evaluating adsorbent regeneration, long-term stability, and system optimization to support large-scale implementation.

Author Contributions

Conceptualization, N.A.H. and N.H.A.; methodology, N.A.H. and N.H.A; software, N.H.A. and N.S.A.; validation, N.A.H., N.H.A., and N.H.M.; formal analysis, N.H.A. and N.H.M.; investigation, N.A.H. and N.S.A.; resources, N.M.A. and N.S.A.; data curation, N.A.H. and N.H.A.; writing—original draft preparation, N.A.H. and N.H.A.; writing—review and editing, N.A.H.; visualization, N.H.M.; supervision, N.A.H. and N.H.A.; project administration, N.H.A. and N.S.A; funding acquisition, N.H.A.. All authors have read and agreed to the published version of the manuscript.

Institutional Review Board Statement

Not applicable.

Informed Consent Statement

Not applicable.

Data Availability Statement

Data supporting the findings of this study are available upon reasonable request from the corresponding author.

Funding

This research was funded by Universiti Tun Hussein Onn Malaysia (UTHM), through Tier 1 [Vot J133] and Geran Penyelidikan Pascasiswazah, GPPS [Vot Q673].

Acknowledgments

The authors are very grateful to Universiti Tun Hussein Onn Malaysia (UTHM) for providing a supportive environment and permission to use their laboratory facilities for this research.

Conflicts of Interest

The authors declare that there is no conflict of interest regarding the publication of the paper.

References

1. Ciesielczuk, T.; Głowacki, M.; Rosik-Dulewska, C.; Poluszyńska, J. Extraction of heavy metals and phosphorus from sewage sludge ashes. *J. Ecol. Eng.* **2025**, *26*, 185-196, https://doi.org/10.12911/22998993/202871.
2. Lan, J.; Liu, P.; Hu, X.; Zhu, S. Harmful Algal Blooms in Eutrophic Marine Environments: Causes, Monitoring, and Treatment. *Water* **2024**, *16*, 2525, https://doi.org/10.3390/w16172525.
3. Abdoli, S.; Asgari Lajayer, B.; Dehghanian, Z.; Bagheri, N.; Vafaei, A.H.; Chamani, M.; Rani, S.; Lin, Z.; Shu, W.; Price, G.W. A Review of the Efficiency of Phosphorus Removal and Recovery from Wastewater by Physicochemical and Biological Processes: Challenges and Opportunities. *Water* **2024**, *16*, 2507, https://doi.org/10.3390/w16172507.
4. El Kaim Billah, R.; Khan, M.A.; Essenni, S.; Achak, M.; Majdoubi, H.; Bahsis, L.; Lima, E.; Jeon, B.-H. A mechanistic insight into anionic phosphate adsorption on developed chitosan.ZnO@metakaolin biocomposite. *Int. J. Biol. Macromol.* **2025**, *308*, 142405, https://doi.org/10.1016/j.ijbiomac.2025.142405.
5. Abdullah, N.H.; Shanmuganathan, R.; Muthusamy, T.; Hui, Y.Z.; Abdul Salim, N.A.; Fulazzaky, M.A.; Hadibarat, T.; Jusoh, M.N.H. Phosphate Adsorption from Aqueous Solution Using Different Mass of Raw

Waste Marsh Clam Shells as an Alternative Novel Adsorber. *Biointerface Res. Appl. Chem.* **2024**, *14*, 114, https://doi.org/10.33263/BRIAC145.114.
6. Liu, L.; Wu, J.; Wu, P.; Wang, T.; Sun, L.; Li, B.; Liu, J.; Liu, S.; Ma, K.; Ye, Q.; Zhu, N.; Dang, Z. Mechanism of coupled phosphate-calcium modulation of nanoplastic transport in porous media: Role of solution chemistry and surface interactions. *Chem. Eng. J.* **2025**, *522*, 167481, https://doi.org/10.1016/j.cej.2025.167481.
7. Nur Atikah Abdul, S.; Zaini, M.A.A.; Fulazzaky, M.A.; Puteh, M.H.; Abdullah, N.H.; Nuid, M.; Lazim, Z.M.; Ahmad, N. A Two-Stage Batch System for Phosphate Removal from Wastewater by Iron-Coated Waste Mussel Shell to Assess the Optimum Adsorbent Dosage. *J. Water Chem. Technol.* **2022**, *44*, 10-20, https://doi.org/10.3103/S1063455X22010088.
8. Shin, Y.S.; Holló, G.; Lagzi, I.; Yang, S.H. Control of Calcium Carbonate Crystallization in an Orthogonal Diffusion System. *Cryst. Growth Des.* **2024**, *24*, 9994-10002, https://doi.org/10.1021/acs.cgd.4c01159.
9. Tan, Z.; Fan, X.; Fan, Q.; Lu, S.; Yu, T.; Ma, L.; Luo, Y.; Li, J.; Li, H.; Hu, Y.-b. Phosphate recovery from aqueous environment with recyclable nanoscale zero-valent iron coated with aluminum hydroxide. *Chem. Eng. Sci.* **2025**, *302*, 120908, https://doi.org/10.1016/j.ces.2024.120908.
10. Katsuura, Y.; Asaoka, S.; Takeda, K.; Nakashita, S.; Hayashi, K.; Tanaka, K.; Inada, Y.; Okuda, T. Adsorptive removal of phosphate from aqueous solutions using iron–lanthanum-doped foam glass adsorbent. *Water Environ. Res.* **2025**, *97*, e70025, https://doi.org/10.1002/wer.70025.
11. Muslim, N.H.; Kamarul Zaman, A.A.; Asmizam, A.S.N.; Norhaizat, D.N.; Abdullah, N.H.; Ngadiman, N.; Abu Hassan, N.; Abdul Salim, N.A.; Fulazzaky, M.A.; Talaiekhozani, A. Recovery of Phosphorus through Different Masses Calcined Chicken Eggshells Adsorbent in Water: Prediction, Kinetic and Isotherm Model. *J. Adv. Res. Micro Nano Eng.* **2024**, *24*, 20-34, https://doi.org/10.37934/armne.24.1.2034.
12. Bbumba, S.; Karume, I.; Nsamba, H.K.; Kigozi, M.; Kato, M. An Insight into Isotherm Models in Physical Characterization of Adsorption Studies. *Eur. J. Appl. Sci.* **2024**, *12*, 115-134, https://doi.org/10.14738/aivp.122.16738.
13. Al-dhawi, B.N.S.; Kutty, S.R.M.; Jagaba, A.H.; Aminu, N.; Birniwa, A.H.; Al-Shawesh, G.A.M.; Almahbashi, N.M.Y.; Al-Yaari, A. Boron adsorption from aqueous solutions through column study: desorption mechanisms, regeneration techniques, and kinetic insights. *Desalin. Water Treat.* **2024**, *320*, 100586, https://doi.org/10.1016/j.dwt.2024.100586.
14. Wang, H.; Luo, H.; Qin, T.; Yang, J.; Chen, L.; Liu, M.; Tang, M.; He, B.-J.; Jing, Z. Recyclable adsorbents of Fe and La co-modified clam shells for phosphorus removal from domestic sewage: Characterization and mechanisms. *iScience* **2025**, *28*, 111762, https://doi.org/10.1016/j.isci.2025.111762.
15. Zhuang, D.; Chen, Z.; Sun, B. Thermal Decomposition of Calcium Carbonate at Multiple Heating Rates in Different Atmospheres Using the Techniques of TG, DTG, and DSC. *Crystals* **2025**, *15*, 108, https://doi.org/10.3390/cryst15020108.
16. Galizia, P.; Tavolaro, A.; Baldisserri, C.; Craciun, F.; Mercadelli, E. Breakthroughs in scanning electron microscopy poling of massive dense and porous lead-free piezoelectric ceramics. *Scr. Mater.* **2025**, *266*, 116795, https://doi.org/10.1016/j.scriptamat.2025.116795.
17. Salim, N.A.A.; Fulazzaky, M.A.; Puteh, M.H.; Khamidun, M.H.; Yusoff, A.R.M.; Abdullah, N.H.; Ahmad, N.; Lazim, Z.M.; Nuid, M. Adsorption of phosphate from aqueous solution onto iron-coated waste mussel shell: Physicochemical characteristics, kinetic, and isotherm studies. *Biointerface Res. Appl. Chem.* **2021**, *11*, 12831-12842, https://doi.org/10.33263/BRIAC115.1283112842.
18. Yusoff, F.M.; Umi, W.A.D.; Ramli, N.M.; Harun, R. Water quality management in aquaculture. *Cambridge Prisms: Water* **2024**, *2*, e8, https://doi.org/10.1017/wat.2024.6.
19. Kassa, A.; Engida, A.; Endaye, M. Eco-friendly adsorbents for industrial dye removal: A comprehensive review of low-cost alternatives. *Desalin. Water Treat.* **2025**, *323*, 101362, https://doi.org/10.1016/j.dwt.2025.101362.
20. Zheng, C.; Yang, X.; Kang, K.; Xie, Y.; Tang, M.; Song, H.; Liang, Y.; Hu, J.; Bai, S. Comparison and development of the descriptive model with polynomial structures to fit multi-component dynamic breakthrough curves with roll-up, stepwise, and saddle-shaped structure. *Sep. Purif. Technol.* **2025**, *355*, 129644, https://doi.org/10.1016/j.seppur.2024.129644.
21. Meina, L.; Qiao, M.; Zhang, Q.; Xu, S.; Wang, D. Study on the dynamic adsorption and recycling of phosphorus by Fe–Mn oxide/mulberry branch biochar composite adsorbent. *Sci. Rep.* **2024**, *14*, 1235, https://doi.org/10.1038/s41598-024-51416-w.
22. González-López, M.E.; Laureano-Anzaldo, C.M.; Pérez-Fonseca, A.A.; Arellano, M.; Robledo-Ortíz, J.R. A

discussion on linear and non-linear forms of Thomas equation for fixed-bed adsorption column modeling. *Rev. Mex. Ing. Quim.* **2021**, *20*, 875-884, https://doi.org/10.24275/rmiq/Fen2337.
23. Fulazzaky, M.A.; Salim, N.A.A.; Puteh, M.H.; Messer, T.; Othman, M.H.D.; Jaafar, J.; Ismail, A.F.; Rahman, M.A. Mechanisms and mass transfer kinetics of Cr(VI) adsorbed by mussel shell incorporated adsorptive membrane. *Desalin. Water Treat.* **2024**, *319*, 100537, https://doi.org/10.1016/j.dwt.2024.100537.
24. Susilawati, S.; Andriayani, A.; Sihombing, Y.A.; Saragi, I.R.; Masruchin, N.; Nuryawan, A.; Irma, M. Study of Ammonium Adsorption Mechanism in Hydrothermalized Pahae Natural Zeolites: Kinetic and Isotherm Adsorption, and Thermodynamics. *Trends Sci.* **2024**, *22*, 8993, https://doi.org/10.48048/tis.2025.8993.
25. Patel, H. Comparison of batch and fixed bed column adsorption: a critical review. *Int. J. Environ. Sci. Technol.* **2022**, *19*, 10409-10426, https://doi.org/10.1007/s13762-021-03492-y.
26. Zhang, X.; Liu, X.; Zhang, Z.; Chen, Z. Removal of phosphate from aqueous solution by chitosan coated and lanthanum loaded biochar derived from urban dewatered sewage sludge: adsorption mechanism and application to lab-scale columns. *Water Sci. Technol.* **2021**, *84*, 3891-3906, https://doi.org/10.2166/wst.2021.485.

Publisher's Note & Disclaimer